Spreading of mercury droplets on thin silver films at room temperature

Avraham Be'er,[1] Yossi Lereah,[2] Aviad Frydman,[1] and Haim Taitelbaum[1]
[1]*Department of Physics, Bar-Ilan University, Ramat-Gan 52900, Israel*
[2]*Faculty of Engineering, Tel-Aviv University, Tel-Aviv 69978, Israel*
(Received 4 January 2007; published 2 May 2007)

We study the spreading characteristics of a reactive-wetting system of mercury (Hg) droplets on silver (Ag) films in room temperature. This is done using our recently developed method for reconstructing the dynamical three-dimensional shape of spreading droplets from two-dimensional microscope images [A. Be'er and Y. Lereah, J. Microsc. **208**, 148 (2002)]. We study the time evolution of the droplet radius and its contact angle, and find that the spreading process consists of two stages: (i) the "bulk propagation" regime, controlled by chemical reaction on the surface, and (ii) the "fast-flow" regime, which occurs within the metal film as well as on the surface and consists of both reactive and diffusive propagation. We show that the transition time between the two main time regimes depends solely on the thickness of the Ag film. We also discuss the chemical structure of the intermetallic compound formed in this process.

DOI: 10.1103/PhysRevE.75.051601 PACS number(s): 68.08.Bc, 68.37.−d, 68.35.Ct

I. INTRODUCTION

The spreading of liquid droplets on solid surfaces [1–5] is an important process in material science, optics, and technology, with a diverse range of applications, such as soldering, typing and painting, gluing, condensation of droplets on solid substrates, and coating of glasses by photoresist liquids in photolithography processes. The classical wetting process is characterized in terms of a contact angle θ between the droplet and the underlying substrate. Theoretical studies [1] assume that for small droplets (where gravity is negligible) and for small angles ($\theta \ll 1$), the droplet has a spherical-cap shape. Under this approximation the evolution in time of the droplet shape is given by

$$H_0(t) = \frac{1}{2} R(t)\theta(t), \tag{1}$$

where $R(t)$ is the droplet radius, $\theta(t)$ is the angle of contact, and $H_0(t)$ is the height at the droplet's center [Fig. 1(a)]. The theoretical and experimental results for $R(t)$ and $\theta(t)$ show that droplet spreading is usually very slow, with power-law scaling like Tanner's law, $R(t) \sim t^{1/10}$ and $\theta(t) \sim t^{-3/10}$ (see [3] for a review).

When a chemical reaction is involved in the wetting process [6–11], the spreading characteristics differ significantly from classical wetting systems. In such reactive-wetting systems, $R(t)$ and $\theta(t)$ do not obey a power law. Moreover, a single function cannot describe the full range of $R(t)$ and $\theta(t)$. Landry and Eustathopoulos [9,10], for example, studied the dynamics of reactive wetting of metallic drops on smooth ceramic surfaces. In their system, a linear spreading regime corresponding to $R(t) \sim t$ was observed for an intermediate part of the spreading process.

The different dynamics in the reactive-wetting systems results from the additional and different mechanisms, which include, for example, the rate and free energy of the reaction, the viscosity and surface tension of the reacting droplet, the wettability of the substrate before and after the reaction, the solubility of the materials, and the surface heterogeneity [6,9].

Due to the complexity of reactive-wetting processes, a general theory for their dynamics is not available [6,8], and the general behavior of $R(t)$ and $\theta(t)$ in reactive-wetting systems throughout the entire spreading process is a long-standing open question. Moreover, it is believed that it would hardly be possible to apply a single model to all these systems. However, despite the diversity of reactive-wetting systems, several common characteristics of the spreading dynamics have been observed. One of these is the existence of several time regimes. In the very early time regime, the velocity is relatively high and the contact angle rapidly decays. The second time regime is when reactive wetting is effective. In this region, the spreading radius grows linearly with time (constant velocity). The contact angle slowly decays or remains more or less constant. In some systems, this region may be divided into two subregions: a transient region and the main steady-state region [9]. In the final regime, the reaction continues through a precursor or a reaction band [7–10]. In this region, the contact angle is constant.

In this work we study the time evolving shape (radius and angle) of a mercury droplet spreading on a silver film. These specific materials, which are relevant, e.g., to dentistry [12,13], have not been studied before in the context of spreading processes. The main advantages of choosing these materials are that the spreading experiment can be performed in room temperature and can be easily observed and monitored using an optical microscope and a 3CCD camera, within relatively reasonable time scales (a few minutes). In a series of papers, we have recently studied the kinetic roughening properties of the interface line of this process [14–19]. In the current work, we show that the spreading in this system consists of several time regimes. The first regime is the propagation of the droplet bulk where the droplet radius grows linearly and the contact angle decreases. This is followed by a fast-flow regime of a precursorlike motion, where the crossover time depends on the thickness of the underlying silver substrate. The fast-flow regime consists of two subregimes, a linear propagation [7], with a velocity signifi-

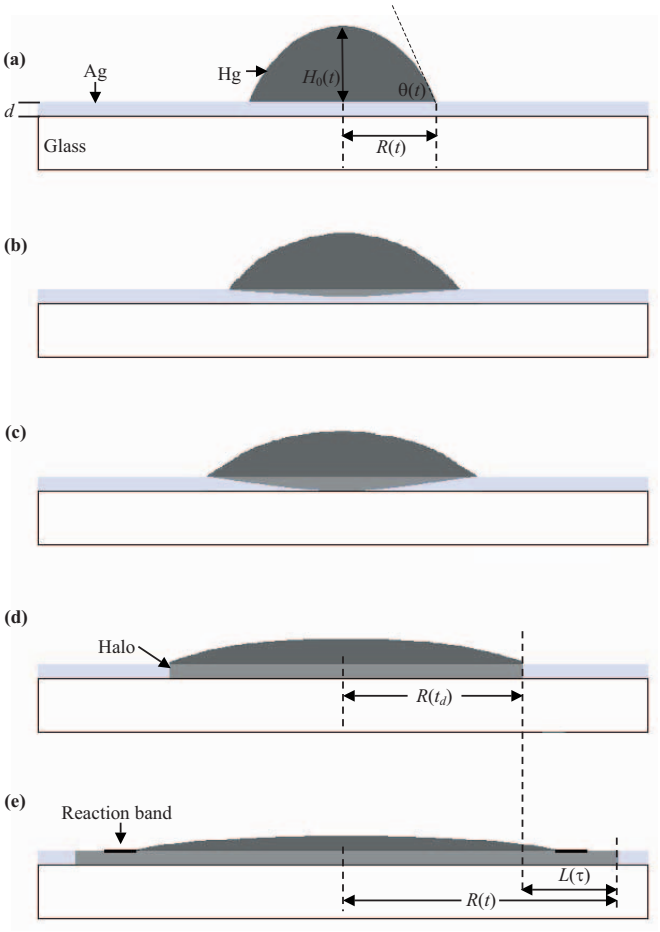

FIG. 1. (Color online) Schematic sequence of mercury droplet spreading on thin silver films in room temperature. (a) Droplet placement on the film. (b) Droplet spreading and reacting with the underlying substrate. (c) Mercury touching the glass. (d) Starting of the fast-flow regime, halo propagation. (e) Final spreading stage.

cantly higher than that of the bulk, which crosses over to a seemingly diffusive motion at the final stages of the process [8,11]. This may be due to different mechanisms, reaction and diffusion, each is dominant in a different subregion.

The main research tool of the current work is our newly developed experimental method [20], which is based on differential interference contrast (DIC) microscopy. It enables one to evaluate the structure of tiny (>1 pL), opaque, and transparent droplets with high temporal (0.04 s) and spatial (1 μm) resolution and with an angle resolution of 1°. With respect to the current study, it has many advantages over other methods for evaluating the three-dimensional shapes of propagating droplets and their precursor films. These methods were discussed in [19] and include interferential techniques [21,22], light reflection [23,24], confocal interference microscopy [25], ellipsometry [26,27], side-view techniques [4,5,7,9], atomic force microscopy (AFM) measurements [28], and the Rame Hart goniometer system [29,30].

The paper is organized as follows. In Sec. II, we present the methodology of our study. Sections III and IV are devoted to a detailed description of the bulk propagation and the fast-flow dynamics, respectively. In Sec. V, we discuss the intermetallic compound formed in the reaction band. The paper is summarized in Sec. VI.

II. METHODOLOGY

A. Experimental setup

We have recently developed a technique [20] which enables one to reconstruct the time-resolved three-dimensional (3D) shape of tiny (10–1000 μm in diameter) objects with high spatial and temporal resolutions. The method is based on quantitative reflected-polarized-light microscope measurements (Axioskop-ZEISS), which are achieved using a DIC accessory. The source light, which is a polarized white light, is split into two partial beams that hit the sample very close to each other (less than 0.5 μm). After hitting the sample, the beams interfere, causing a colored pattern image due to the difference in the optical path length between them. The two-dimensional images provided by the optical microscope consist of different colors, which indicate different slopes in the specimen structure. The color spectrum is calibrated so that each color corresponds to a specific slope (angle) of the mercury droplet. The measurements were taken in a given diametric cross section of the droplet, parallel to the beam-splitting direction.

The advantages of this technique are as follows: (i) Ability to follow *in situ* changes at a high time resolution of 0.04 s between successive video frames. (ii) A high spatial resolution of 1 μm. The resolution limitation is due to the wavelength of the incident microscope light and the digitization of the captured frames. (iii) Angle resolution of ~1°, resulting in a vertical resolution of ~0.02 μm. (iv) Very small volumes (down to 1 pl) are accessible, an improvement over other methods which are limited to larger droplets. (v) The technique enables one to analyze both opaque and transparent droplets. (vi) The 3D reconstruction process is achieved from a top view, enabling one to observe the entire triple line, its velocity, its roughness, and its growth during the process. Thus, the radius and the angle can be measured simultaneously. In addition, top view increases the experiment's accuracy by averaging over the entire two-phase surface boundary of the drop.

B. Materials

In this paper, we use this method to study the time evolution of the 3D shape of small Hg droplets, with initial diameter of 150 μm, which spread on thin Ag films at room temperature. This experiment involves chemical reactions between the solid and the liquid, which create intermetallic compounds such as Ag_3Hg_4 and Ag_4Hg_3 [12], that may influence the spreading dynamics. The experiments were performed for various film thicknesses (2000, 3000, 3500, 3800, 4200, 5000, and 6000 Å). The Ag thin films were thermally deposited on microscope slides in a vacuum chamber. Since the dynamics is dramatically affected by the Ag oxidation [14], the experiments were performed shortly after the Ag evaporation.

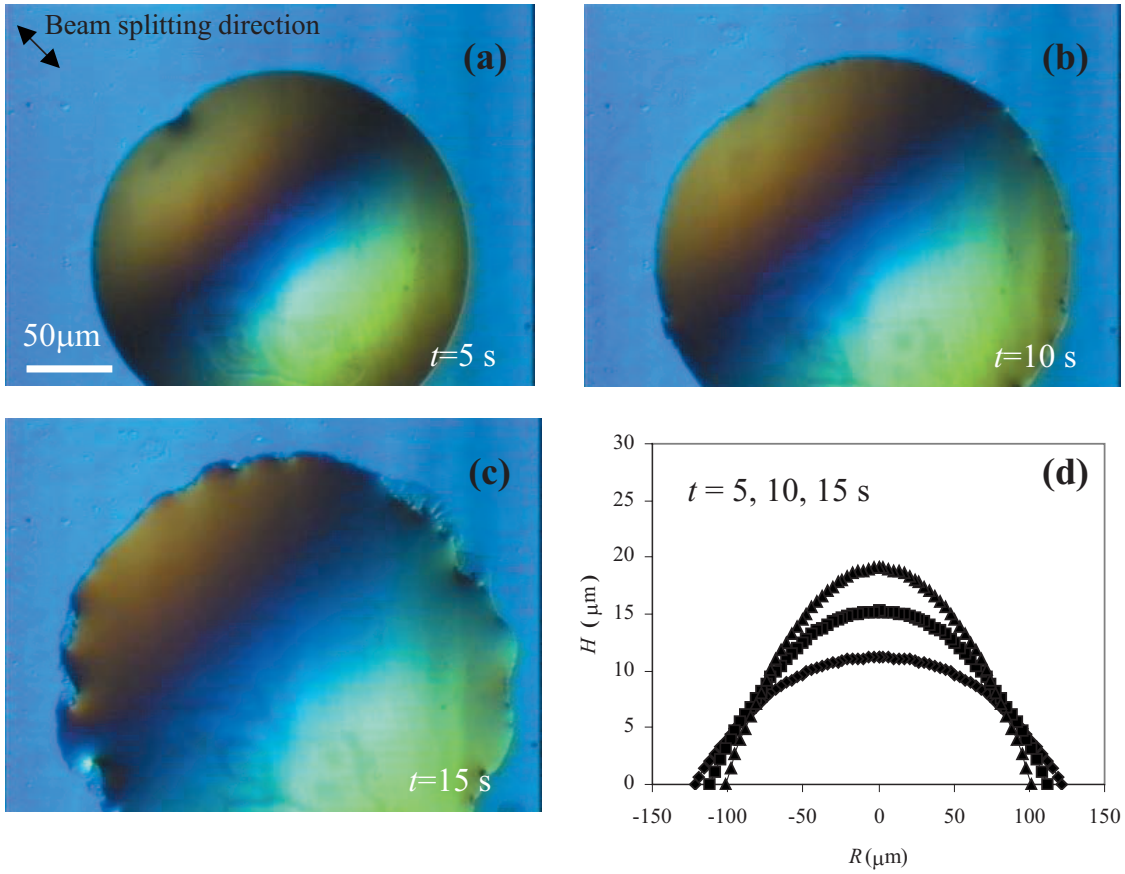

FIG. 2. (Color online) (a)–(c) Top-view DIC-light-microscopy pictures of Hg droplet spreading on a 4200-Å-thick Ag film, taken at times 5, 10, and 15 s, respectively. The droplet initial diameter, prior to deposition, is 150 μm. (d) Dynamical side view of the droplet shape, reconstructed from the top-view pictures (a)–(c). The measurements were taken in a given diametric cross section of the droplet, parallel to the beam-splitting direction, shown in (a).

III. BULK PROPAGATION

The first stage in the spreading process is what we call the "bulk propagation" regime, which lasts for several seconds, depending on the thickness of the Ag film. In this regime, upon placing the droplet on the Ag layer [Fig. 1(a)], the mercury bulk starts to spread [Fig. 1(b)] , circularly symmetric, with a smooth contour line. In Fig. 2, we show the top-view results for a typical sample of thickness 4200 Å. The pictures of Figs. 2(a)–2(c) were taken at times 5, 10, and 15 s, respectively. The colors indicate different slopes in the specimen; e.g., the blue at the background and at the droplet's top represents 0° and the orange at the interface of (c) (t=15 s) represents 15°. The colors evolve with time, indicating the dynamic 3D changes. The seemingly nonradially symmetric color in Figs. 2(a)–2(c) is due to the fact that measurements are performed along a given cross section of the droplet, the beam-splitting direction, shown in Fig. 2(a). For the same reason, the measurements are not affected by the overall roughening of the droplet edge. The top-view light-microscope pictures were transformed into projected side views using the above-mentioned technique. The droplet shape reconstruction is plotted in Fig. 2(d).

In Fig. 3, we show the results for the radius $R(t)$ and the angle $\theta(t)$ for the same data of Fig. 2. It is shown that, initially, the droplet radius grows linearly, $R(t) \sim t$, implying a motion of constant velocity, in this case of 2.1 μm/s [Fig. 3(a)], and the angle of contact $\theta(t)$ decreases continuously [Fig. 3(b)]. At about t=15 s, $\theta(t)$ demonstrates a sudden step in its decreasing trend. As will be shown later, this is the time when the mercury crossed the entire silver layer for the first time and touched the underlying glass [Fig. 1(c)]. Hence, we define this characteristic time as t_d, where d is the thickness of the Ag layer. The constant velocity remains approximately the same, with a very slight variation at t_d. In Figs. 4 and 5, we show the same behavior for other silver thicknesses, 2000 and 6000 Å, where the characteristic time t_d is 3.2, and 32 s, respectively.

Interestingly, the velocity of the bulk propagation is approximately the same for all Ag thicknesses (2000, 3000, 3500, 3800, 4200, 5000, and 6000 Å), having the average value of 2.5±0.4 μm/s. It is reasonable to assume that the velocity does depend, however, on the reaction of the mercury with the silver surface. Indeed, when the silver film is exposed to air prior to the mercury spreading process, the velocity is different, since silver oxidation takes place only on top of the Ag layer [14,18]. It turns out that this surface velocity is much higher (about two orders of magnitude) than the mercury-silver reaction rate *inside* the silver film. For example, in the 4200-Å system, since the mercury crosses

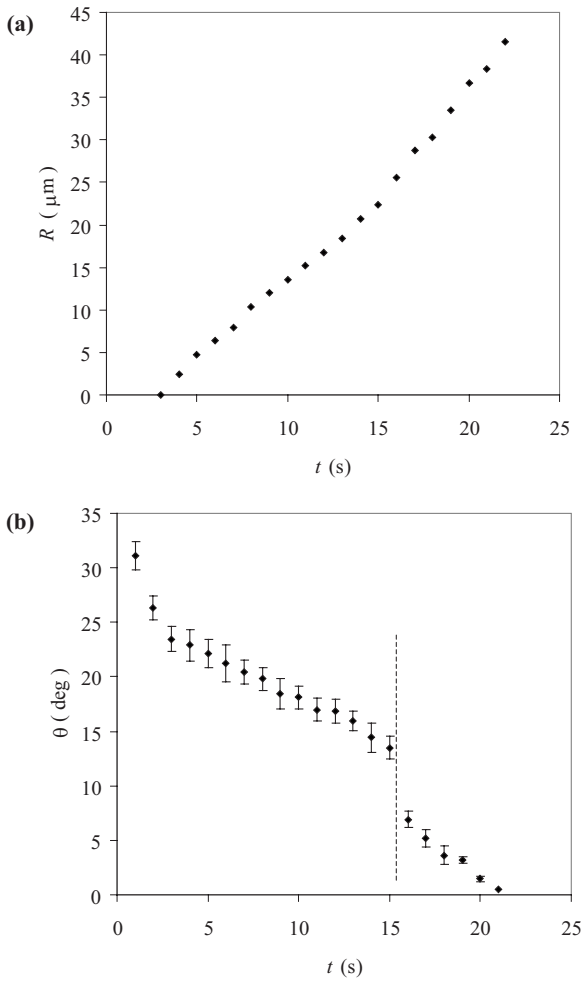

FIG. 3. (a) The radius $R(t)$ and (b) the angle $\theta(t)$ as a function of time for the bulk propagation regime for silver thickness of 4200 Å. The interface constant velocity is 2.1 μm/s. At t_d=15 s, $\theta(t)$ demonstrates a sudden step in its decreasing trend.

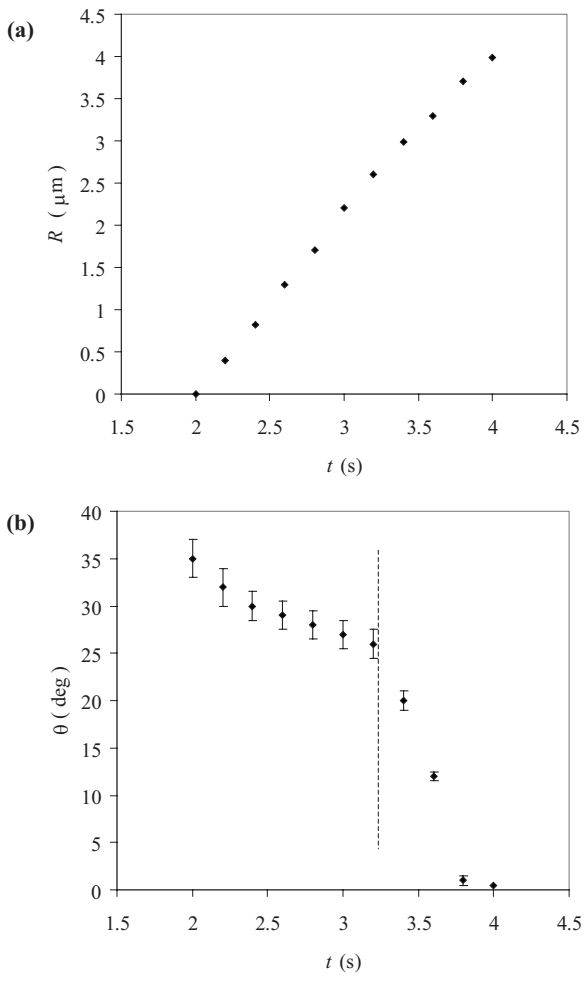

FIG. 4. (a) The radius $R(t)$ and (b) the angle $\theta(t)$ as a function of time for the bulk propagation regime for silver thickness of 2000 Å. The interface constant velocity is 2 μm/s. At t_d=3.2 s, $\theta(t)$ demonstrates a sudden step in its decreasing trend.

the silver thickness in 15 s, the averaged perpendicular velocity is (4200 Å)/(15 s)=0.028 μm/s, which is two orders of magnitude smaller than the horizontal velocity 2.1 μm/s. A possible interpretation is that the reaction inside the film is attenuated by another physical mechanism, possibly diffusion. In Fig. 6(a), we show the dependence of t_d on the thickness d, averaged over ten different samples for each thickness. The results support a square dependence of this characteristic time scale on the thickness length scale, which indeed supports the conjecture that the reaction of the mercury inside the silver film is diffusion limited.

In Fig. 6(b), we show the dependence of the angle θ_d in which the new front detaches from the bulk, on the silver film thickness. This figure shows that the angle strongly depends on the thickness, which rules out the naive assumption that the new front detachment has to do with a certain critical angle of the silver bulk.

The bulk propagation regime does not terminate at t_d, but rather extends further in time. However, t_d is the time when another regime, the fast-flow dynamics, shows up.

IV. FAST-FLOW DYNAMICS

At time t_d, a new spreading regime, which we call the "fast-flow regime," occurs abruptly. In this regime, a new and thin front (~500 Å in height, verified by AFM), which optically looks like a halo, detaches from the bulk and flows ahead with a much higher velocity (Fig. 7). We define the propagation distance of this halo as $L(\tau) \equiv R(t) - R(t_d)$, where $R(t)$ and $R(t_d)$ are the distances from the center of the droplet at times t and t_d, respectively, and $\tau \equiv t - t_d$ [see Figs. 1(d) and 1(e)]. We found that $L(\tau)$ exhibits a crossover behavior in time (Fig. 8), starting from a linear regime $L(\tau) \sim \tau$ at the earlier times (on the τ scale), followed by a $\tau^{0.4}$ behavior at later times, when the spreading process is slowing down. In the first, linear, reaction-dominated regime, the thickness-dependent velocity is constant, having the values 140, 110, and 40 μm/s, for the 2000, 4200, and 6000 Å thicknesses, respectively. The second regime seems to be diffusion dominated, with the same time exponent (0.4) for all silver thicknesses (Fig. 8), although the prefactor is different for each case. Similar crossover behaviors between reaction-dominated to diffusion-dominated processes on the surface

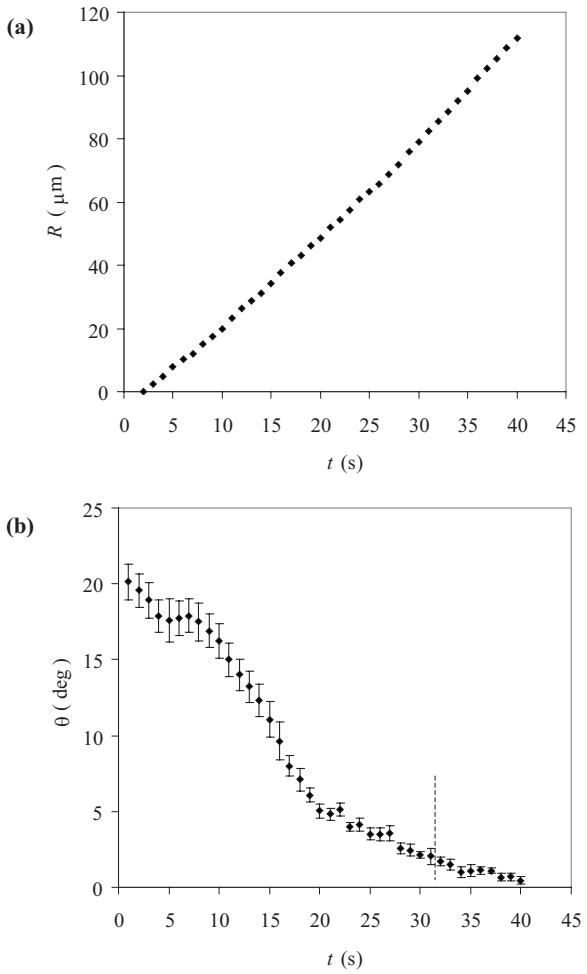

FIG. 5. (a) The radius $R(t)$ and (b) the angle $\theta(t)$ as a function of time for the bulk propagation regime for silver thickness of 6000 Å. The interface constant velocity is 2.9 μm/s. At t_d=32 s, the droplet touches the glass but the sudden step in the decreasing trend of $\theta(t)$ is not visible as the angle is already very small (2°).

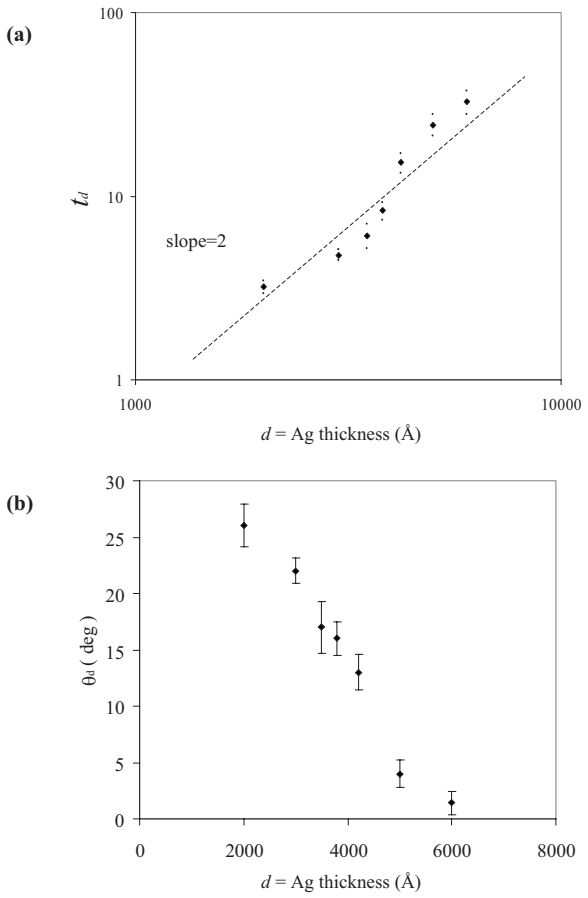

FIG. 6. (a) Log-log plot of the dependence of t_d on the thickness d, as obtained from experiments performed with silver thicknesses 2000, 3000, 3500, 3800, 4200, 5000, and 6000 Å, each averaged over ten different samples. The results seem to follow a slope of 2, supporting a diffusion-limited reaction inside the silver film. (b) The dependence of the angle θ_d, in which the new front detaches from the bulk, on the silver thickness, for the same thicknesses as in (a). The angle strongly depends on the thickness.

were reported in [8,11]. The 0.4 exponent is slightly far from the 0.5 time exponent in standard diffusion, but may still represent a diffusion regime (see also Fig. 7 in [8]). Alternatively it may reflect a subdiffusive motion (time exponent less than 0.5) whose origin is yet to be studied. The velocity of the halo propagation was found to be significantly higher (one to two orders of magnitude) than the velocity in the bulk spreading regime.

The fact that the formation of the faster thin layer that flows ahead of the nominal contact line depends on the Ag thickness leads us to assume that the glass beneath the Ag film is an important factor in the fast-flow regime. Therefore, we looked at the Ag film from the *bottom* (the glass slide side). We found that the observed thin Hg layer runs also between the silver and the glass (beneath the silver) in the same structure and velocity that it apparently runs on top. Figures 9(a) and 9(b) show the interface between the mercury and the silver (4200 Å thickness in this case) of the same frame of the specimen from both sides. The similarity between the two pictures is remarkable. We rule out the possibility that the observed thin Hg front, looking from the bottom, is just the projection of an Hg layer that runs on the

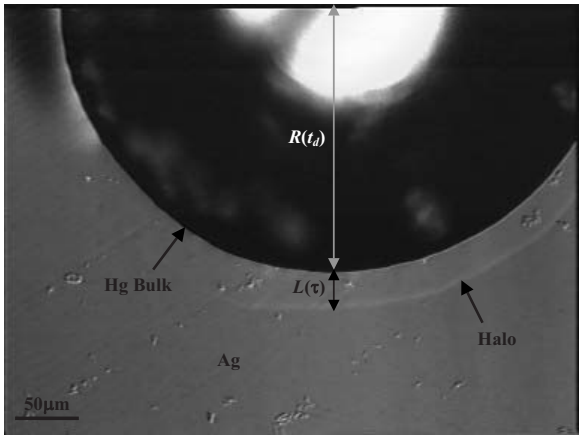

FIG. 7. A top-view, DIC-light-microscopy image of the thin front, which detaches from the bulk and looks like a halo, for Ag thickness of 2000 Å. Since this image was taken only 7 TV frames (~0.3 s) after the detachment, $L(\tau)$ is still quite small compared to $R(t)$. The bulk advancement during this time interval is negligible.

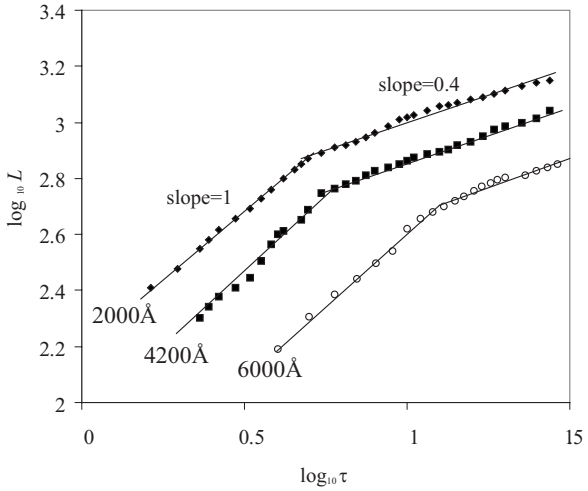

FIG. 8. The propagation of the halo for three different Ag thicknesses. For each thickness, τ is set to be 0 at a different time, depending on the specific t_d. For all cases, $L(\tau)$ exhibits a crossover behavior in time, starting from a linear regime $L(\tau) \sim \tau$ at the earlier times (on the τ scale), followed by a $\tau^{0.4}$ behavior at later times. The velocities at the earlier times are 140, 110, and 40 μm/s, for the 2000, 4200, and 6000 Å thicknesses, respectively.

surface, because no light (of the incident source light) could cross the opaque Ag layer. This observation led us to sketch Figs. 1(d) and 1(e) with the reaction all over the thin film.

Looking from the bottom side, we measured the time it takes the droplet to cross the Ag layer down to the glass. Surprisingly, we found it to be exactly t_d. This leads us to suggest that the formation of the new front and the sudden step in $\theta(t)$ are related to the fact that the droplet has crossed the Ag layer and touched the glass. As the droplet reaches the glass it is not constrained anymore by the surface reaction, because no reaction exists between the Hg and the glass. Consequently, it flows fast through the Ag layer in order to

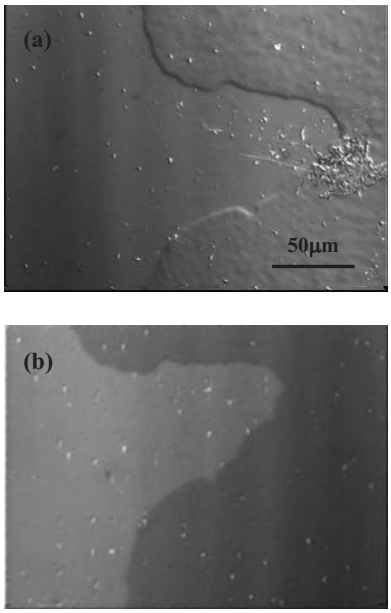

FIG. 9. The similarity between (a) top view and (b) bottom view of the mercury-silver interface in the 4200-Å silver thickness case.

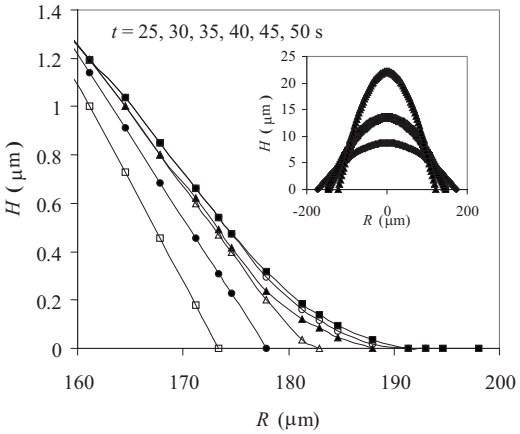

FIG. 10. A typical concave to convex transition in a 6000-Å sample, obtained using our technique [20]. The cross section of the droplet shape is presented for times 25, 30, 35, 40, 45, and 50 s, and the concave-convex transition takes place between t=30 and 35 s (t_d=32 s). Inset: the macroscopic cross section of the bulk before the transition, at times 5, 15, and 25 s.

lower the entire system energy. This observation can explain the thickness dependence of the halo velocity at this time regime (Fig. 8).

Recall that the shape of the droplet was found to be spherical-cap-like during the entire first spreading regime. However, as the new front starts to flow and the macroscopic contact angle drops dramatically, the bulk contact with the substrate becomes concave rather than convex. A typical concave to convex transition in the 6000-Å sample, obtained using our new technique [20], is shown in Fig. 10. The cross section of the droplet shape is presented for times 25, 30, 35, 40, 45, and 50 s, and the concave-convex transition takes place between t=30 and 35 s (recall that t_d=32 s for this system). We have chosen to show the 6000-Å system in which the transition occurs while the contact angle is almost 0°, in order to demonstrate the capability of our technique.

V. REACTION BAND: INTERMETALLIC COMPOUND

The fast-flow dynamics gives rise to the formation of a reaction band [8–10], which starts within the fast-flow time regime. A typical reaction band in our system is shown in Fig. 11. This band was observed only on the top surface [see Fig. 1(e)] but not from the bottom view. This band is apparently due to the growth of a new intermetallic phase on top of the film. Scanning electron microscopy (SEM) studies [14] suggest that the new intermetallic compound is Ag_4Hg_3. It grows in a structure of islands that can be explained by nucleation and growth mechanisms. Its average growth velocity in the spreading direction was found to be that of the bulk propagation, namely about 2.5 μm/s.

VI. SUMMARY

In this work we studied the spreading of a mercury droplet on a thin silver film in room temperature. We analyzed the various time regimes of this reactive-wetting system through the time evolution of the radius and the contact angle of the

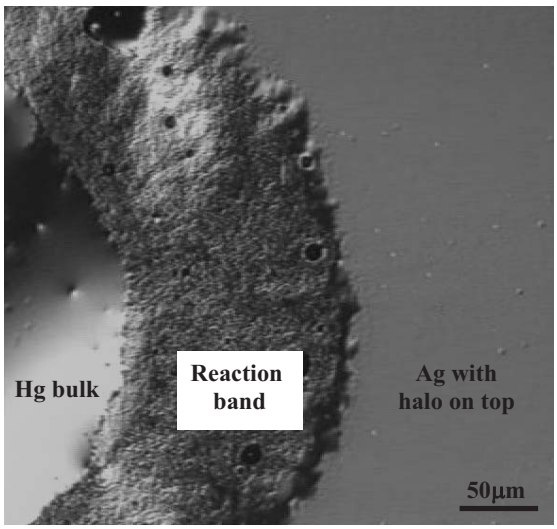

FIG. 11. A typical snapshot of the reaction band formed between the mercury bulk and the silver film with the halo already on its top. Silver film thickness is 4200 Å.

droplet. These parameters were followed using a microscopy technique of side-view reconstruction from top-view images. We looked at the film thickness effect on these parameters, and in particular we observed a remarkable rapid halo propagation, which was observed not only from a top view but also from a bottom view. This propagation eventually crosses over to diffusivelike growth, due to surface diffusion dominancy at the final stages of the reactive wetting. In addition, we discussed the nature of the chemical reaction between the mercury and the silver in this system.

In future work, we plan to study the effect of patterned silver surface on the dynamical properties of the system. This would involve lithography techniques. In addition, we plan to study the effect of temperature changes using an appropriate heating stage.

ACKNOWLEDGMENT

We thank the Israel Science Foundation (ISF) for financial support, Grant No. 1342/04.

[1] P. G. de Gennes, Rev. Mod. Phys. **57**, 827 (1985).
[2] L. Leger and J. F. Joanny, Rep. Prog. Phys. **55**, 431 (1992).
[3] A. Oron, S. H. Davis, and S. G. Bankoff, Rev. Mod. Phys. **69**, 931 (1997).
[4] M. J. de Ruijter, J. De Coninck, T. D. Blake, A. Clarke, and A. Rankin, Langmuir **13**, 7293 (1997).
[5] M. J. de Ruijter, J. De Coninck, and G. Oshanin, Langmuir **15**, 2209 (1999).
[6] C. D. Bain and G. M. Whitesides, Langmuir **5**, 1370 (1989).
[7] F. G. Yost, F. M. Hosking, and D. R. Frear, *The Mechanics of Solder-Alloy Wetting and Spreading* (Van Nostrand Reinhold, New York, 1993).
[8] H. K. Kim, H. K. Liou, and K. N. Tu, J. Mater. Res. **10**, 497 (1995).
[9] K. Landry and N. Eustathopoulos, Acta Mater. **44**, 3923 (1996).
[10] N. Eustathopoulos, Acta Mater. **46**, 2319 (1998).
[11] Y. M. Liu and T. H. Chuang, J. Electron. Mater. **29**, 405 (2000).
[12] M. Hansen, *Constitution of Binary Alloys*, 2nd ed. (McGraw-Hill, New York, 1958).
[13] M. Levlin, E. Ikavalko, and T. Laitinen, Fresenius' J. Anal. Chem. **365**, 577 (1999).
[14] A. Be'er, Y. Lereah, and H. Taitelbaum, Physica A **285**, 156 (2000).
[15] A. Be'er, Y. Lereah, I. Hecht, and H. Taitelbaum, Physica A **302**, 297 (2001).
[16] A. Be'er, Y. Lereah, A. Frydman, and H. Taitelbaum, Physica A **314**, 325 (2002).
[17] A. Be'er, I. Hecht, and H. Taitelbaum, Phys. Rev. E **72**, 031606 (2005).
[18] A. Be'er, M.Sc. thesis, Bar-Ilan University, Ramat-Gan, Israel, 2000.
[19] A. Be'er, Ph.D. thesis, Bar-Ilan University, Ramat-Gan, Israel, 2005.
[20] A. Be'er and Y. Lereah, J. Microsc. **208**, 148 (2002).
[21] I. C. Callaghan, D. H. Everett, and A. J. P. Fletcher, J. Chem. Soc., Faraday Trans. 1 **79**, 2723 (1983).
[22] R. Aveyard, J. H. Clint, D. Nees, and V. Paunov, Colloids Surf., A **146**, 95 (1999).
[23] C. Allain, D. Ausserre, and F. Rondelez, J. Colloid Interface Sci. **107**, 5 (1985).
[24] D. Ausserre, A. M. Picard, and L. Leger, Phys. Rev. Lett. **57**, 2671 (1986).
[25] D. G. Fischer and B. Ovryn, Opt. Lett. **25**, 478 (2000).
[26] E. G. Bortchagovsky and L. N. Tarakhan, Phys. Rev. B **47**, 2431 (1993).
[27] F. Heslot, A. M. Cazabat, and P. Levinson, Phys. Rev. Lett. **62**, 1286 (1989).
[28] S. S. Sheiko, A. M. Muzafarov, R. G. Winkler, E. V. Getmanova, G. Eckert, and P. Reineker, Langmuir **13**, 4172 (1997).
[29] X. H. Wang and H. Conrad, Scr. Metall. Mater. **30**, 725 (1994).
[30] X. H. Wang and H. Conrad, Scr. Metall. Mater. **31**, 375 (1994).